Global J. Environ. Sci. Manage. 8(3): 297-314, Summer 2022, Serial #31

Global Journal of Environmental Science and Management
(GJESM)

Homepage: https://www.gjesm.net/

ORIGINAL RESEARCH ARTICLE

Soil classification in a seismically active environment based on join analysis of seismic parameters

Y. Asnawi[1,2,3], A. V.H. Simanjuntak[3,4], U. Muksin[3,*], M. Okubo[5], S.I. Putri[3], S. Rizal[1], M. Syukri[1]

[1] *Graduate School of Mathematics and Applied Sciences, Universitas Syiah Kuala, Banda Aceh 23111, Indonesia*

[2] *Universitas Islam Negeri Ar-Raniry, Banda Aceh 23111, Indonesia*

[3] *Tsunami and Disaster Mitigation Research Center, Universitas Syiah Kuala, Jl. Prof. Dr. Ibrahim Hasan, Gampong Pie, Indonesia*

[4] *Meteorological, Climatological, and Geophysical Agency, BMKG, Banda Aceh 23234, Indonesia*

[5] *Natural Science Cluster, Science and Technology Unit, Kochi University, Akebono-cho Kochi, Japan*

ARTICLE INFO

Article History:
Received 16 September 2021
Revised 25 October 2021
Accepted 02 December 2021

Keywords:
Earthquake
Seismic amplification
Seismic wave velocity
Spatial autocorrelation
Spectral ratio

ABSTRACT

BACKGROUND AND OBJECTIVES: Soil or rock properties where buildings are situated play an important role in the ground shaking caused by an earthquake. The highly populated Banda Aceh city in the northernmost Sumatra is flanked by two active faults, the Seulimeum and the Aceh segment. Therefore, it is crucial to investigate the subsurface characteristics of the region to reduce the earthquake risk as there was no regional study has been conducted so far.
METHODS: Characteristics of the soil or rock of the subsurface were derived from various seismic parameters. The seismic microtremors were recorded at 36 sites covering the highly populated city and the two active faults. The spatial autocorrelation method was used to obtain a dispersion curve based on the relationship between seismic frequencies and phase velocity from triangular geophones array to determine the shear wave velocity of the subsurface layer. The seismic amplification, dominant frequency and vulnerability value at each measurement point were measured using the horizontal-to-vertical spectral ratio method. The maps of velocity structure and HVSR parameters were generated from the interpolation of those seismic parameters.
FINDINGS: Based on the variation of the four geophysical parameters: shear wave velocity, seismic amplification, dominant frequency, and seismic vulnerability, the study area can be clustered into five different groups: I) Banda Aceh, II) Jantho, III) Krueng Raya, IV) Lhoknga-Lhoong, and V) Seulawah, which classify the different types of rocks. The classification of soil properties from the combination of shear wave and horizontal-to-vertical spectral ratio data correlates with the geology of the study area.
CONCLUSION: The Banda Aceh city, flanked by the two active faults, is characterized by low shear wave velocity and high amplification because the city stands on the sedimentary basin; thus, it requires a detailed investigation prior to constructing infrastructures. The other clusters are located on the relatively less vulnerable areas, indicated by moderate shear wave velocity and moderate to low seismic vulnerability indexes. The joint analysis shows that the combination of physical properties, including the shear wave velocity, seismic amplification, and dominant frequency, can be used to investigate lithology and seismic vulnerability into a specific cluster. The research results are essential for hazard mitigation and can be used for disaster risk management by the local government. A detailed investigation with denser measurement points needs to be conducted to comprehensively describe the types of rocks in Banda Aceh and its surrounding.

DOI: 10.22034/gjesm.2022.03.01

©2022 GJESM. All rights reserved.

NUMBER OF REFERENCES	NUMBER OF FIGURES	NUMBER OF TABLES
51	8	1

*Corresponding Author:
Email: *muksin.umar@unsyiah.ac.id*
ORCID: 0000-0001-7297-8065

Note: Discussion period for this manuscript open until October 1, 2022 on GJESM website at the “Show Article”.

INTRODUCTION

Seismic amplification and soil properties based on seismic shear wave velocity parameters are crucial to investigate, particularly seismically active and highly populated regions. Banda Aceh and its surrounding areas in the northernmost Sumatra are among the most earthquake-prone zones because they are surrounded by earthquakes sources (Fig. 1). Large offshore earthquakes (e.g. the Mw 9.3 Sumatra–Andaman earthquake and the Mw 8.5 Nias earthquake) mainly occur along active subduction zones. Meanwhile, onshore earthquakes tend to occur along the northern segment of the Sumatra Fault System, including the Aceh fault, Seulimeum fault (Sieh and Natawidjaja, 2000), Pidie Jaya fault (Muzli *et al.*, 2018; Idris *et al.*, 2019) and Central Aceh fault (Muksin *et al.*, 2019). The Seulimeum fault generated an earthquake with a magnitude of M 7.0 in 1936, and such an event caused building collapse and severe property damage, along with several reported fatalities (Untung *et al.*, 1985). Although no major event has been recorded in the last 170 years along the Aceh segment, the occurrence of a large earthquake remains possible (Ito *et al.*, 2012). Therefore, mitigation plans for earthquake events in Banda Aceh should be prioritized. The city is one of Sumatra's most economically developed areas and is becoming a highly populated region. Bilham (2009) suggested that rapid development has put developed cities at relatively high risk for a significant increase in fatalities and economic losses caused by damages to buildings or other infrastructure in the coming years. Earthquake intensity and construction quality play an important role in building damages. Several geophysical parameters can extend infrastructure damages, including seismic amplification, ground acceleration, rock or soil properties of sites, and geology of regions (Goda *et al.*, 2015). Seismic amplification, which represents the possible extent of ground shaking of sites during earthquakes, can be defined by the maximum value of the horizontal-to-vertical spectral ratio (HVSR) at a certain dominant frequency (Nakamura, 1997). Areas with high damage ratios during earthquake events have high values of HVSR and low dominant frequencies (Nakamura, 1997).

Several studies have shown that the types of soils or rocks can be classified based on the velocity of shear waves (Vs) passing through the subsurface. Very dense soil has Vs values between 360 and 760 m/s, whereas soft soil has Vs values of less than 180 m/s. Several methods can be used to determine Vs values, including multichannel surface wave analysis (Park *et al.*, 2007) and the less invasive method, called spatial autocorrelation (SPAC) (Cho *et al.*, 2004; Cho, 2019). For regional studies, shallow structures can be derived by ambient noise tomography (Ryberg *et al.*, 2016), while the seismic refraction of very localized areas can be used to determine the velocity of pressure (Vp) and shear waves (Vs). Among the methods, SPAC is one of the least expensive ones, but it remains reliable when applied to inaccessible areas, such as the Banda Aceh region in the northernmost Sumatra. Some successful SPAC research around the world includes those conducted in Nevada (Scott *et al.*, 2006), Italy (Forte *et al.*, 2019), and Japan (Matsuoka *et al.*, 2006). The objective of the research is to investigate the geophysical properties of the shallow and vulnerability of the northernmost Sumatra. The Vs values are used to derive the types of soil based on the classification of the National Earthquake Hazards Reduction Program (NEHRP). The combination of various HVSR data, including seismic amplification and dominant frequency and Vs values, can be used to derive more detailed soil clusters in the northernmost Sumatra. The results can be used to investigate the probabilistic seismic hazards of Banda Aceh and update the loss assessment map of Banda Aceh developed by Rusydy *et al.* (2020) for different earthquake model scenarios.

Geology of study area

A complex tectonic process makes Banda Aceh and its surrounding areas prone to moderate–large earthquakes that potentially generate massive ground shaking on the surface. Such shaking is attributed to the Banda Aceh basin, formed since the Quaternary and pre-Quaternary and recognized as alluvium deposited. The Banda Aceh basin is mostly influenced by recent alluvium and marine sediment products consisting of gravel, sand, silt, and clay (Rusydy *et al.*, 2020). The upper layer of the southeastern part of the Banda Aceh basin is covered by pre-Quaternary rocks from Pliocene to Pleistocene (Fig. 1) up to 500 m; these rocks consist of calcareous and tuffaceous sandstones (Siemon and Steuer, 2010). As a result of oblique subduction, the Banda Aceh basin is flanked by the Aceh fault in the southwest and the Seulimeum

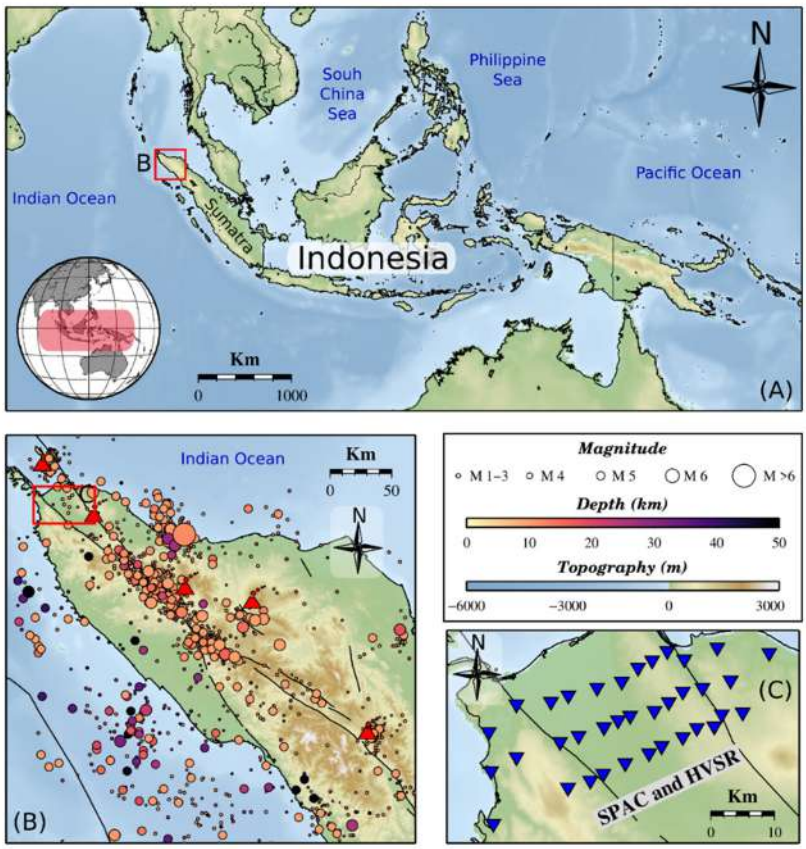

Fig. 1: (a) Geographical map of Indonesia and the study area in the Aceh Province. (b) Seismic activities map of Aceh Province showing earthquake distribution that mostly occurred along active faults and subduction zones. The red square marks the study area for this study in the Banda Aceh city and its surrounding. (c) The Study area in the Banda Aceh city and its surrounding and the observation points (blue triangle) while Aceh fault in the left part and Seulimeum fault in the right part (black line).

fault in the northeast (Muksin *et al.*, 2019). The Aceh fault marks the boundary between the Banda Aceh basin and the limestone formed from Jurassic to Cretaceous as an oceanic accretion rock that is part of the Woyla group (Barber *et al.*, 2005). In addition, the Seulimeum fault was formed within the volcanic Quaternary in the northwest of the Krueng Aceh basin (Siemon and Steuer, 2010). Therefore, Culshaw *et al.*, (1979) categorized this basin as a graben-type structure.

A previous study conducted by Asrillah *et al.*, (2019) indicated that the soil properties beneath the Banda Aceh basin have a Vs structure that generally dips down from SE to NW and gradually declines from SW to NE. This result may be affected by the soil type around the Seulimeum fault being denser than that around the Aceh fault, as also related to geology. As shown in Fig. 2, the geological structure in the Banda Aceh basin is dominantly formed by young alluvium sediments that can amplify ground shaking on the surface. With sandbar formations and material structures with a low density, Banda Aceh and Aceh Besar are likely to be earthquake- and liquefaction-prone zones. The current study aims to investigate the physical properties of the subsurface of the northernmost Sumatra. This study was carried out in Aceh Besar and Banda Aceh region in 2020.

MATERIALS AND METHODS

Data Acquisition

The experiment was conducted at 36 measurement points in the northernmost Sumatra

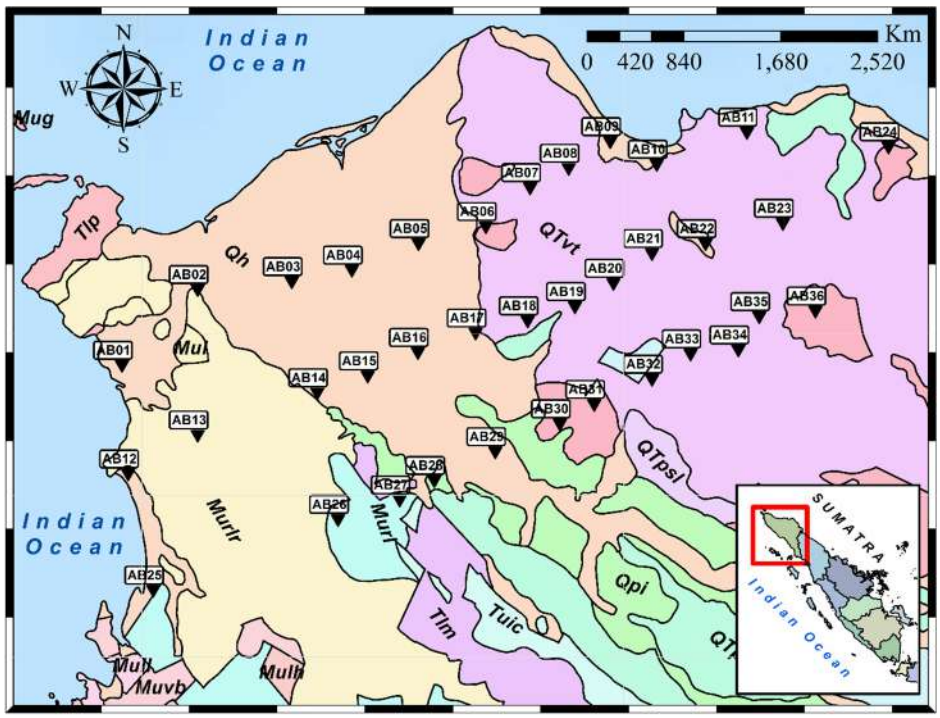

Fig. 2: Geological map of Banda Aceh and Aceh Besar regency (modified Barber et al., 1998). Most materials around the study area are composed of young alluvium (Qh), volcanic rocks (QTvt) and limestone (Murl) from the Cenozoic until the Tertiary. Measurement points are at 36 locations around Banda Aceh and Aceh Besar cross the Sumatran and Seulimeum faults, with the distance between each site being 5–10 km

covering the Banda Aceh city, the sedimentary basin and the Seulimeum and the Sumatran faults (Fig. 2). The measurement of microtremors using center-less triangle seismic arrays was performed using three high sensitivity geophones (80 V/m) with a natural frequency of 5 Hz and operating temperature range of −40 °C–80 °C. The instrument has a harmonic distortion of less than 0.1% and can thus reduce the problems caused by the overheating and overloading of power system equipment. The distance between sites was 5–10 km, and the data recording time for each site was 30–45 min. The geophones were set with a distance of 3 m as the center-less curricular array (Cho *et al.*, 2006); therefore, the array radius was 2.6 m. The sampling rate in the DSS Cube as the data logger was set to 100 sps (samples per second), and the effective resolution was set to 22 bits; at this condition, the recording of interval stability and time accuracy lasted 0.01 ms. Recordings were made by placing three one-component geophones at azimuths of 0°, 120°, and 240° into three-component (north–south, east–west, and vertical) channels of DSS Cube as the data logger. To derive the classification of rocks and soils, the data from the recordings were used to determine the shear velocity (Vs) beneath the measurement points based on the SPAC method. At the same locations, microtremors were also used by a Nanometrics trillium compact broadband seismometer with a sensitivity of 750 V/m ± 0.5%. The seismic waveforms were stored in DSS Cube. The recording was performed for 40 min for each site at a sampling rate of 100 sps. The data were used to determine the amplification and dominant frequency of the sites, as well as the value of seismic vulnerability, based on the HVSR method. These parameters represent the vulnerability of buildings or areas to be affected by earthquakes.

Vs modeling using SPAC

The SPAC method is used to obtain a dispersion curve (curve of frequency vs. phase velocity) and model the shear wave velocity structure (Vs) in the

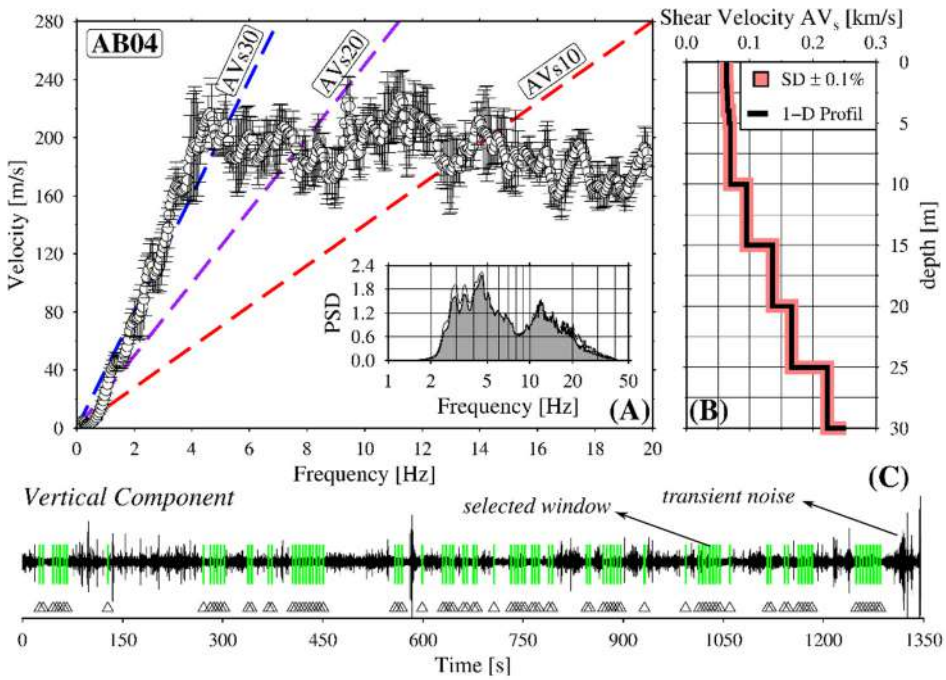

Fig. 3: (a) Dispersion curve of microtremors recorded at site AB09 describing the relationship between frequency and velocity following the linear trend ($AVs_{1\text{-}10}$ (blue), $AVs_{11\text{-}20}$ (purple), and $AVs_{21\text{-}30}$ (red)). The AVs trend at a specific depth (10, 20, and 30 m) was set based on the average value in the thick layer at a shallow depth. (b) AVs was converted with Eq. 3 to obtain Vs as the representative value for a specific depth. The graph shows a three-layer graph formed by Vs over depths of 10, 20, and 30 m. (c) Example of waveform recording in the vertical component at AB09 and the segmentation window (green triangle)

subsurface layer based on microtremors (Thein *et al.*, 2015). A microtremor is assumed to be complex mixed waves consisting of Rayleigh waves that arrive from multiple directions to the field (Okada, 2006). Therefore, the accuracy of microtremor analysis is highly dependent on the shape and size of arrays. Such dependence is avoided by conducting microtremor array surveys using circular seismic arrays with a certain distance. In the SPAC method, observation records are transformed into the Fourier domain, and the autocorrelation function of each geophone is calculated. Autocorrelations calculated from a triangular array configuration are referred to as SPAC functions, useful in estimating dispersion curves, which help obtain subsurface structures under realistic conditions. In the current work, BIDO2.0 tool (Cho, 2019) was used to estimate the dispersion curve of the recorded microtremor data (Fig. 3a). The recorded data were filtered, with a range of 0.1–10 Hz. For the spectral analysis of microtremors, the recorded data were divided into 10.24 s segments (Fig. 3b) to avoid transient noise from civilian and machine activities near the measurement points. The segments containing significant data variations were removed from the calculation based on the short-term average–long-term average (STA/LTA) ratios (Fig. 3c). Selected quiet segments were used to calculate the power spectra and then smoothed by fitting the parzen windows with a bandwidth of 0.3 Hz. The SPAC coefficient was calculated by averaging all azimuths. A root-solving method combining the bisection and secant methods was applied to average the spectra ratio by fitting the Bessel function to search for the radius times the wavenumber rk and the parameter of the Bessel functions in the range [0, rk_{max}]. The value of rk_{max} corresponded to the first maximum or minimum function value. The obtained rk was used to calculate the phase velocity (c) using Eq. 1.

$$c = 2\pi \frac{f}{k} \quad (1)$$

Where, f is the frequency and k is the wavenumber. Given these parameters, the SPAC coefficient, averaged spectra ratio, and dispersion curve were calculated using the BIDO2.0 tool. In general, dispersion forms when waves propagate in the layers of soil and subsurface rocks with different velocity values. The crossing point between a dispersion curve and a surface wavelength proportional to the array radius and frequency represents the phase velocity of the corresponding wavelength (Fig. 3a). Thus, the averaged phase velocity (AVs) of the layered subsurface was obtained in this work. For example, AVs_{30} is the AVs between 0 m (surface) and 30 m. The average shear wave velocities for depths of 0–10 m, 11–20 m, and 21–30 m, labeled respectively as AVs_{10}, AVs_{20}, and AVs_{30}, are obtained when Rayleigh wave velocities correspond to the wavelengths of 13 m, 25 m, and 40 m (Cho *et al.*, 2008). The method has limited accuracy but effectively visualizes the relative spatial variations in shear wave velocities. In this research, three averaged velocity values were estimated: AVs_{10}, AVs_{20}, and AVs_{30}, for each site. With these values, Vs structure of the three-layer subsurface interval velocities can be determined using Eqs. 2, 3 and 4.

$$Vs_{(0-10\,m)} = AVs_{10} \tag{2}$$

$$Vs_{(11-20\,m)} = \frac{(AVs_{11} \cdot AVs_{20})}{(2 \cdot AVs_{11} - 2.AVs_{20}} \tag{3}$$

$$Vs_{(21-30\,m)} = \frac{(AVs_{21} \cdot AVs_{30})}{(3 \cdot AVs_{21} - 2 \cdot AVs_{30})} \tag{4}$$

The Vs values of the layers can be then compared with data from Tohari *et al.* (2015) who assessed the Vs values below stratum using the Cone Penetration Test.

Horizontal to Vertical Spectral Ratio

The HVSR has routinely been considered a quick tool to assess possible amplification effects in seismic hazard studies. The microtremor records in the time domain of the horizontal and vertical components were transformed into the frequency domain to obtain the horizontal and vertical spectra. The current work used the method by Nakamura (1989) involving the HVSR of the single station microtremor records. Generally, the amplitude of a vertical component does not change significantly, whereas that of a horizontal component is affected by soil properties. Vertical components cannot be amplified around frequency ranges, in which horizontal components receive large amplification (Nakamura, 2000). Nakamura (2000) assumed that the horizontal-to-vertical (H/V) spectrum as a frequency function is closely related to the site transfer function of shear waves and that the HVSR represents one of the amplification factors. The different H/V values for the three locations indicate the variations of the site conditions representing the rock properties of the area. In Nakamura's method (Nakamura, 1989, 2000), the local effect arising from surface geology is calculated by the spectral ratio of the horizontal and vertical components (i.e., HVSR) using Eq. 5.

$$\frac{H}{V} = \frac{\sqrt{NS^2 + EW^2}}{V} \tag{5}$$

Where, NS is the spectrum amplitude of the north–south component, EW is the east–west component, and V is the vertical component. The amplitude of the horizontal component (NS and EW) was averaged using the root mean square equation and subsequently divided by the amplitude of the vertical component to obtain the average H/V spectrum. From the H/V spectrum, the dominant frequency and period (f and T) were obtained, as well as the H/V peak, associated with the amplification (A) at each measurement location. The dominant frequency is closely related to the lithological conditions and thickness of the subsurface. Low dominant frequency values are associated with thick layers of soft sedimentary sub surfaces, whereas high dominant frequencies are related to thin subsurface layers (Gallipoli *et al.*, 2004; El-Hady *et al.*, 2012). The high value for a dominant period (low dominant frequency) is due to the thick layer of sediments in the subsurface that trap Rayleigh waves for long periods (Stanko et al., 2017). The H/V spectrum is mostly influenced by wave speed and rock density. If the wave speed is low, the H/V value is high. Furthermore, the amplification value is large for areas composed of low-density rocks or soil. Seismic surface waves propagate slowly in soft sediments, and ground shaking can be amplified and thereby cause severe damage. The seismic vulnerability index (K_g) can be calculated by dividing the square of the

amplification by the dominant frequency value using Eq. 6 (Nakamura, 1989).

$$K_g = \frac{A^2}{F} \quad (6)$$

The Kg value is used to identify soft soil regions and qualitatively estimate possible damage areas (Gosar, 2007; Beroya-Eitner *et al.*, 2009; Asten *et al.*, 2014; Pamuk *et al.*, 2018). Many researchers have used the HVSR method to characterize soil resonance frequency and calculate the vulnerability parameters used for earthquake mitigation plans (Tün *et al.*, 2016; Maresca *et al.*, 2018; Alamri *et al.*, 2020).

RESULTS AND DISCUSSION

Shear wave velocity

An example of the recorded data and the 1D velocity modelling for site AB09 is shown in Fig. 3. The microtremor data were bandpass filtered, with a frequency of 0.1–10 Hz and segmented into several 10 s windows. All segments were converted into the frequency domain using fast Fourier transform to obtain the dispersion curve (Fig. 3a) for the measurement point of AB09. Phase velocity is inversely proportional to frequency, increasing over depth. The dispersion curve for site AB09 shown in Fig. 3 reflects the average shear velocity (AVs) controlled by the frequency range depending on the physical properties of rocks at a depth of 30 m. The relationship between AVs and frequency suggests the vertical heterogeneity of the structure beneath the site. The difference values of the shear wave velocity at all points indicate the lateral heterogeneity of the rocks in the subsurface at a depth of 30 m.

The AVs value at a depth of 20–30 m was 180 m/s (5.9 Hz), while that at 10–20 m is 160 m/s (7.7 Hz). The increasing value of AVs over certain depths suggests increasingly compact rocks or soil in deep layers. Given the average velocity AVs, the shear wave velocity Vs at a certain depth can be determined using Eq. 3. The values of Vs of 100, 160, and 200 m/s at depths of 10, 20, and 30 m, were obtained respectively. The example of Vs beneath site AB09 is shown in Fig. 3b. The graph of Vs is more representative than that of AVs as it shows the increase of Vs at certain depths. The Vs values were interpolated in the vertical and horizontal directions to observe the structure beneath the study area for further analysis. The thickness of the sedimentary layer and the identification of the geological structure can be investigated from the vertical cross section shown in Fig. 4. Three vertical slices showing the structure of the subsurface are provided. Parallel lines crossing the Sumatran and Seulimeum faults were chosen to differentiate the lithologies along the lines. The type of soil along the A-B profile at a depth of 1–10 m with a Vs range of 80–100 m/s is considered as class E soil (Table 1). At greater depths, the soil is classified as class D soil. The Banda Aceh basin can also be seen beneath profiles C–D and E–F in Fig. 4.

The thickness of the sedimentary layer and the identification of the geological structure can be investigated from the vertical cross section in Fig. 4. Three vertical slices showing the structure of the subsurface were presented. Parallel lines crossing the Sumatran and Seulimeum faults differentiate the lithologies along the lines. The type of soil along the A-B profile at a depth of 1–10 m with a Vs range of 80–100 m/s is considered class E soil while at the greater depths, the soil is classified as class D soil (Table 1). The sediment formation of the Banda Aceh basin can also be seen beneath profiles C–D and E–F in Fig. 4 with a similar range. The Vs_{30} figure that is vital for earthquake hazard analysis was presented. The Vs_{30} are different in each station due to the subsurface condition. In Fig. 5, the 1-D velocity model ranges higher to the active fault while lower to the central part.

Fig. 5 shows the lateral variation of the Vs_{30} values between 200 and 240 m/s. The high value of Vs_{30} (between 215 and 220 m/s) is located along the high elevation in the Sumatran fault. The lowest value of Vs_{30} is located in the Banda Aceh basin at 210 m/s (Fig. 4).

Seismic vulnerability

The seismic records were used with minimal transient effect by applying the anti-triggering STA/LTA, with a minimum threshold of 0.1–0.5 s and a maximum threshold of 1.5–2.0 s. After reducing the transient effect in the evaluation stages, a bandpass filter, with a range of 0.005–20 Hz with a 5% cosine taper, was used. The time domain microtremors were converted to frequency domain ones and then windowed using the Konno–Ohmaci method (1998) with b = 40 bandwidth. The spectral ratio graphics

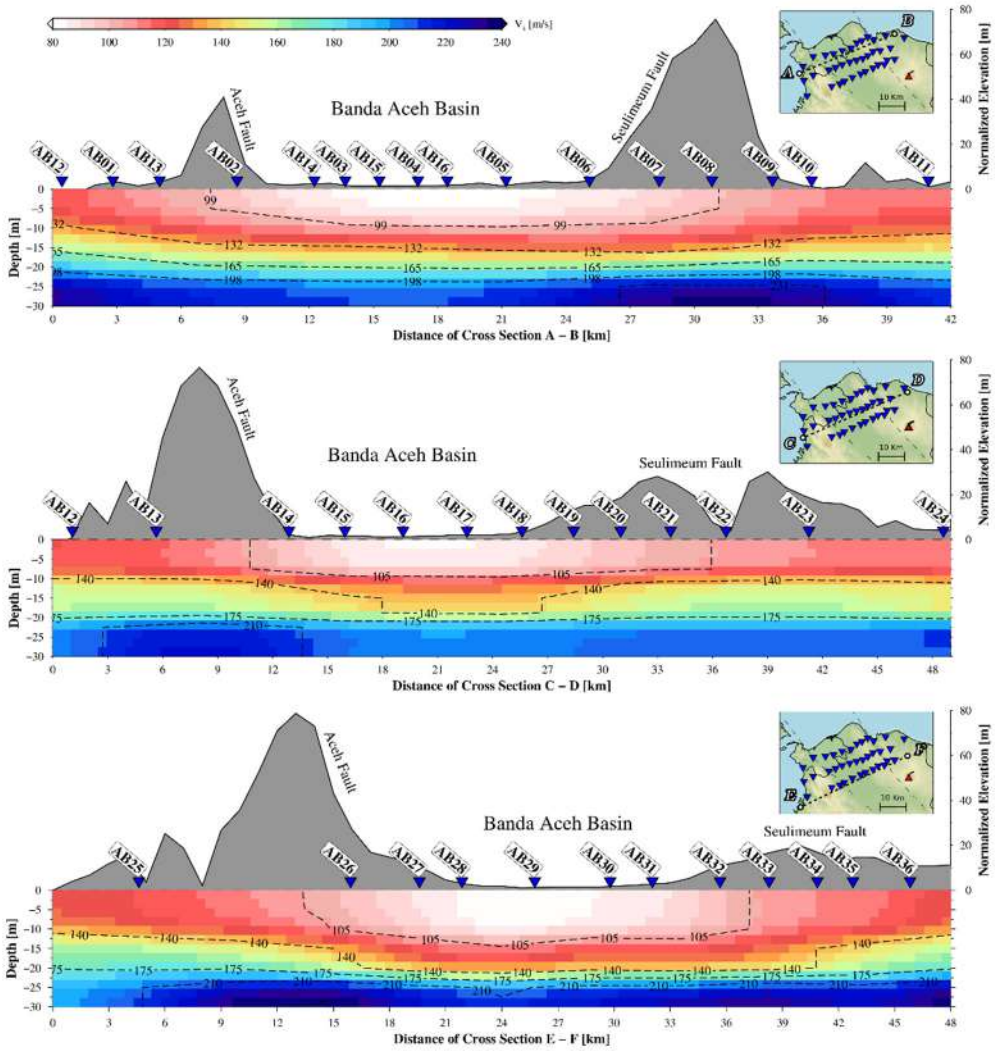

Fig. 4: Three slices are set up to figure the vertical profile of Vs over depth along lines (a) A–B, (b) C-D, and (c) E-F, respectively. The vertical profiles clearly show the existence of the Banda Aceh basin that stand on alluvial sediment in the central part, while the Aceh and Seulimeum fault stand on limestone and volcanic structure in the left and right part

Table 1**:** Five clusters classified from different geophysical parameters (the geological map is considered to define the possible types of rocks)

Cluster	Amplification (A)	Frequency (f)	Vs30	Soil class	Possible types of rocks
I	Low–Moderate	Moderate–High	High	E–D	Young Alluvium
II	Moderate	Low–Moderate	Low	D	Alluvial Sediment
III	High	Low–Moderate	Low	E	Young Alluvial Sediment
IV	Moderate	Moderate	Moderate	D	Limestone
V	Low	High	High	C	Volcanic Rock

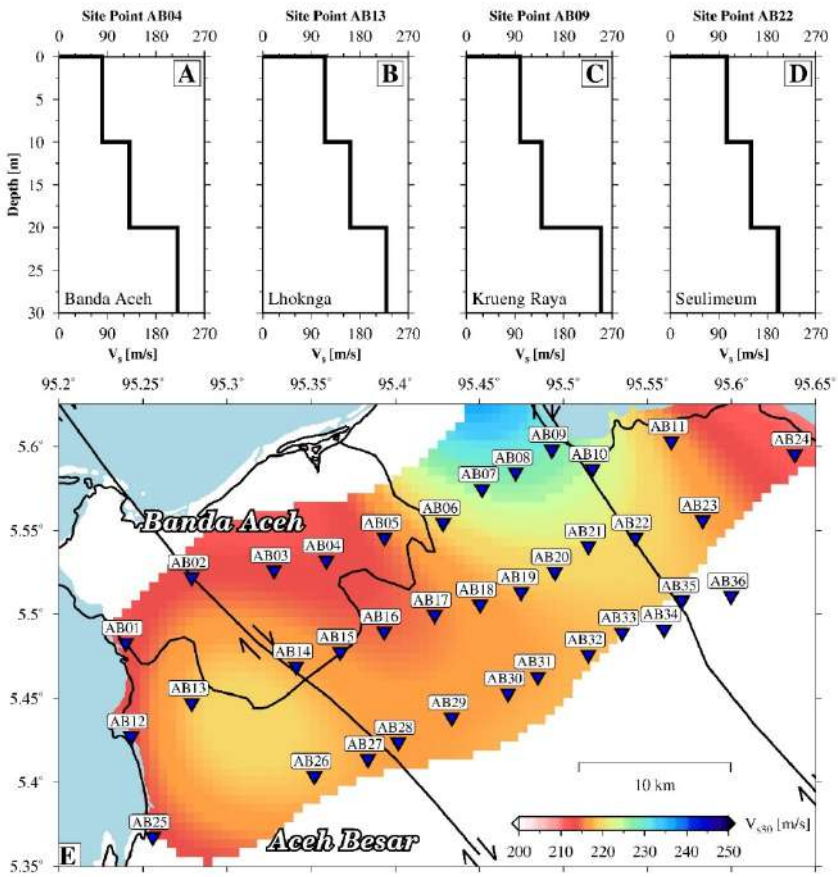

Fig. 5: (a) Examples of 1D velocity model derived from microtremor data obtained by SPAC beneath four sites AB04, AB13, AB09, and AB22; and (b) horizontal profile view of Vs30 as a result of the interpolation of Vs values at all locations

were then obtained by calculating the ratio of the horizontal components to the vertical components as the H/V amplitude. Three examples of microtremor recorded at different locations (along the Sumatran fault, Seulimeum fault, and Banda Aceh basin) and the results of the HVSR analysis are shown in Fig. 6. The different H/V values for the three locations indicate the variations of the site conditions depending on the rock properties of the area.

After analyzing the data from all sites, the values were compiled and the dominant period (T) and vulnerability index (K_g) were calculated. The maps of the dominant frequency and period, the H/V values, and the vulnerability index are provided in Fig. 7. High dominant frequencies were recorded along the Sumatran and Seulimeum faults, while low frequency microtremors were recorded in the Banda Aceh basin of the study area (Fig. 7). In contrast to dominant frequencies, low dominant periods were observed along the faults (Fig. 7b). The authors also calculated the amplification value (A) (Fig. 7c) from the vertical axis of the peak of the H/V curve. Low H/V values were found along the two main faults because hard rocks constituted the areas. Meanwhile, the Banda Aceh basin was characterized by high values of amplification; thus, the seismic vulnerability K_g was also high. As shown in Fig. 7, the highest value of K_g is located in the basin area, while the values of K_g along the two active faults are relatively low.

Statistically, all geophysical properties from HVSR and SPAC analysis can be analyzed to measure the correlation between those parameters, as shown in Fig. 8. Each square provides the correlation values between the variables on each axis, ranging from -1 to +1. The small correlation coefficient (closer to zero) means no linear trend between the two variables,

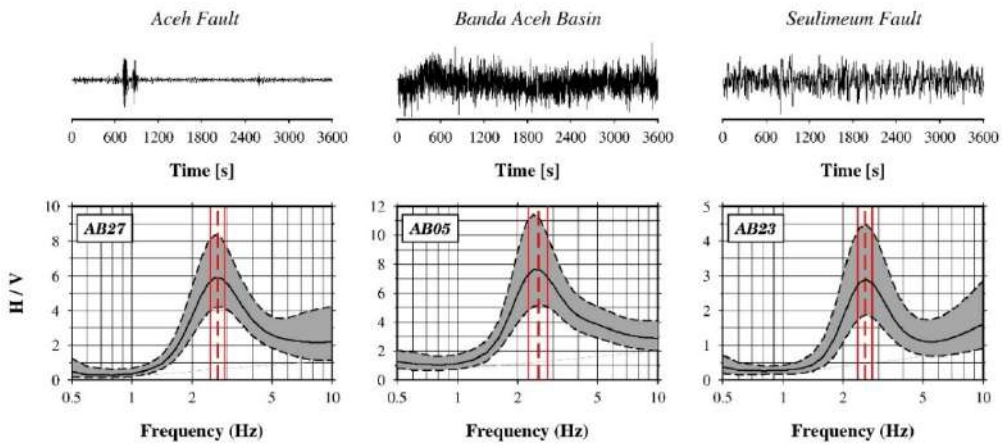

Fig. 6: Three recording examples in AB27, AB05, and AB23 show different waveforms depending on site properties. The spectrum analysis of AB27, AB05, and AB23 generated a normal curve graph of amplitude (A) and frequency (f)

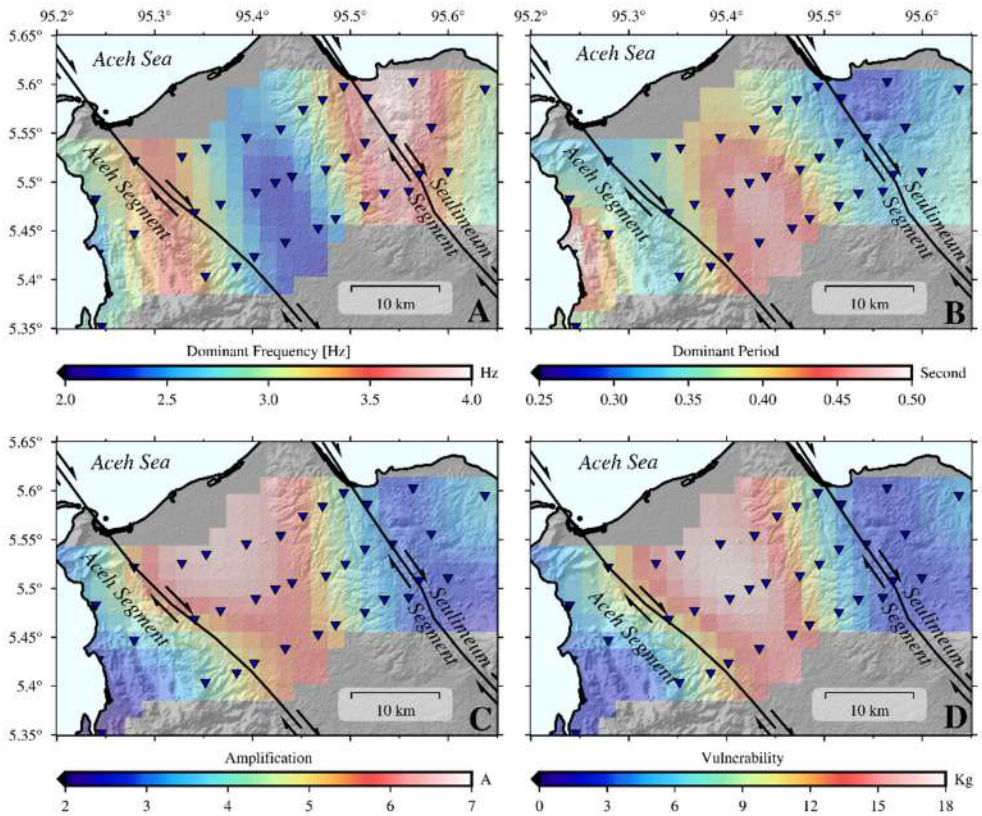

Fig. 7: Maps of (a) dominant frequency, (b) dominant period, (c) amplification, and (d) vulnerability index resulting from HVSR analysis

while the closer to 1 correlation value indicates a positive correlation between the two parameters. The values closer to -1 also indicate a good correlation between parameters. The frequency parameter strongly correlates to shear wave velocity at a depth of 20 m but almost independent seismic amplification.

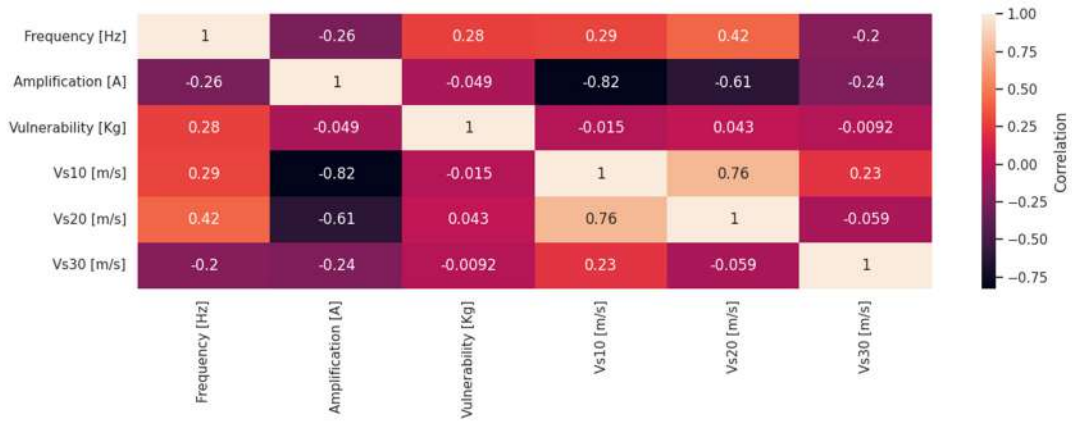

Fig. 8: Correlation index of seismic parameters: frequency, amplification, vulnerability, and shear wave velocities

The amplification has a weak relationship with shear wave velocity at a depth of 10 m. The vulnerability positively correlates to frequency and shows no correlation to shear wave velocity (Vs).

General interpretation of physical properties

The soil or rock characteristics were derived from the geophysical parameters of dominant frequency, amplification, and shear velocity. The authors connected Vs_{30} with the H/V parameters to classify the soil properties into different categories, following the recommendation from the 1997 NEHRP; (Boore, 2004). The clustering results showed different soil classes: soft soil (E), rigid soil (D), and soft rock (C), as specified in Table 1. In most sites, nearly uniform Vs values of over 200 m/s in the third layer (21–30 m) were found, regarded as a more compact and steadier structure than the upper layer.

The soil or rocks at certain depths were considered stiff, given high values of Vs (Fig. 4). Such structures are classified as the class D. The Vs value of the third layer at a depth of 30 m, i.e., Vs_{30}, is important because it is often used in geotechnical investigations. It highlights the characteristics of rocks at a depth of 30 m. The results of the SPAC and H/V analyses indicate a reciprocal relationship between the different geophysical parameters. The area was clustered based on different geophysical properties, Vs_{30}, amplification, and dominant frequency (Fig. 9). The area with physical properties of low Vs_{30}, high amplification, and relatively high dominant frequency was called Cluster I, and the rock type was classified as class E. Clusters II and III had Vs_{30} values between 210 and 228 m/s with a relatively low amplification of 2.5–6. The area with amplification between 2–3, Vs_{30} between 230–244, and dominant frequency of 3–4 Hz was called Cluster IV. Cluster V had the highest values of Vs_{30} between 250–265 and, thus, the highest density; it also had the lowest amplification values and was considered the least seismically prone area. The maps of the clusters in Fig. 7 are shown in Fig. 9 to discuss the seismic soil properties of each area.

Cluster I (Banda Aceh)

Cluster I, where Banda Aceh is located (Fig. 9), is the most important area in this study because it is a densely populated region and is the center of economic and governmental activities. Banda Aceh, standing above the basin, is predominantly composed of alluvium (Fig. 2). This soil type correlates with low Vs, high amplification, and low dominant frequency (Fig. 8). The interpolation of Vs from the first slice A–B shown in Fig. 4 indicates the existence of the Banda Aceh basin and two active faults in the northern part of the study area. Asrillah *et al.* (2019) also profiled the top layer of the Banda Aceh basin as less dense with soft soil and slightly flat layered sediments. The less-dense soil at the top surface is associated with the young alluvium (Qh) suggested by Barber (1998) in the geological map (Fig. 2). From the Cone Penetration Test data, Tohari *et al.* (2015) suggested that the topsoil layers in Banda Aceh mainly consists of clay and sand, coinciding with low shear wave velocity found by this study. During the 2004 Sumatra–Andaman tsunami, many reports raised a possible liquefaction phenomenon in Banda Aceh.

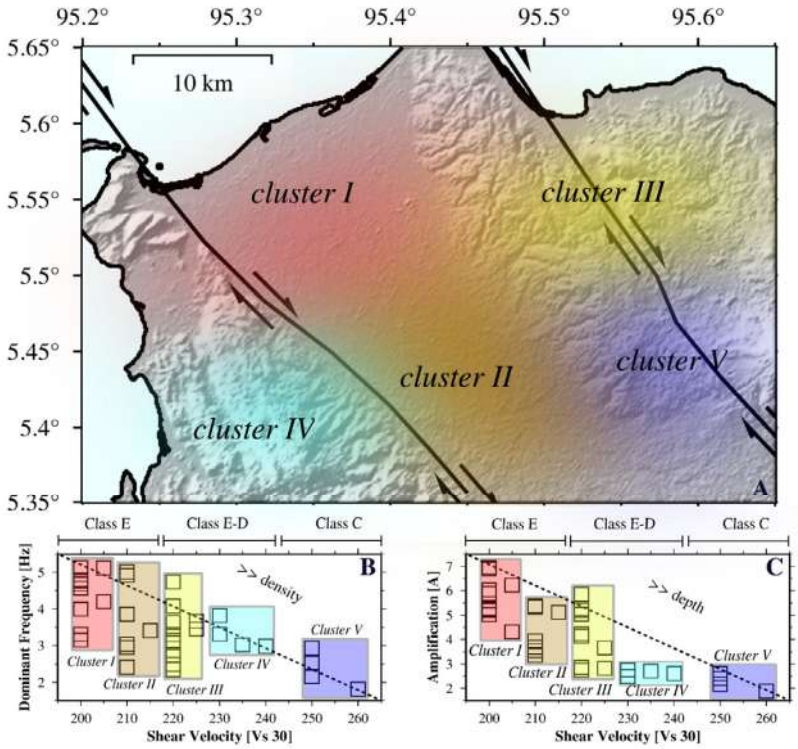

Fig. 9: Clusters of zonation derived from the combination of Vs_{30}, dominant frequency and amplification (A). There is five clusters specifically located by different parameters, Cluster I in the Banda Aceh Basin, called the Banda Aceh cluster, Cluster II in the southern part of Basin Aceh, called the Jantho cluster, cluster III in the northern part of Seulimeum fault, called the Krueng Raya cluster, cluster IV along Aceh fault, called the Lhoknga-Lhoong cluster, and cluster V along Seulimeum fault and Mount Volcano of Seulawah Agam, called the Seulawah cluster

Meanwhile, seismic activities from the two closest active faults, namely, Aceh and Seulimeum, can cause shock effects. Large earthquakes along the two faults with high intensity can potentially cause liquefaction in Banda Aceh (Jalil *et al.*, 2020). Rusydy, *et al.* (2020) analyzed whether an earthquake with Mw 7.0 can cause massive structural damage throughout Banda Aceh; if such an earthquake occurs during the day, their estimates showed a fatality rate of 3.5%–20% of the total population in buildings in general and economic losses reaching thousand million USD.

Cluster II (Jantho)

Jantho Cluster (Cluster II) is characterized by low Vs_{30} and high seismic amplification. The soil and rocks in this area consist of a variety of sedimentary and rock structures, such as the Idi Formation (Idi), Lam Teuba Volcano Formation (QTvt), Seulimeum Formation (QTps), Jantho Complex Formation (Tuic), Meucampi Formation (Tim), and Alluvium Formation. These various formations are due to the cluster location in the complex of the meeting point of the Aceh and Seulimeum faults. This cluster's soil material has been formed since the Late Jurassic to the Holocene because it is incorporated in the Seulawah and Lhoknga–Raba structures. The amplification value is moderate, while the frequency is in the low–moderate range. Vs_{30} is low because the material predominantly contains alluvial sediments but is denser than the same material in the Banda Aceh cluster. This cluster is also located in the same basin as Banda Aceh, and the soil is categorized class D (Tabel 1). The measurement results in this cluster prove the existence of the Banda Aceh basin in the southern part up to the meeting point of the Aceh and Seulimeum faults.

Cluster III (Krueng Raya)

The Krueng Raya cluster is located at the northernmost part of the Seulimeum fault, close to the coastline. The area's rock formation has been formed since the Pleistocene–Holocene with three different formations: Young Alluvium (Qh), Lam Teuba Volcanic (QTvt), and Seulimeum Formation (QTps). The volcanic rock material in this cluster mainly influences the surface profile and other eruption products, such as lahar and pyroclastic flows. The parameter results indicate that the soil group in this cluster is class D, given the moderate amplification value, dominant frequency, and Vs_{30}. In 1936, the northern part of the Seulimeum fault generated an earthquake with a magnitude of M 7.0, causing the collapse and damage of several buildings and leading to several fatalities in the Lam Teuba district. Thus, the vulnerability index is moderate, meaning that a building must match the dominant period (~0.3 s). Furthermore, the cluster has the exact topographical contours as the Lhoknga-Lhoong cluster with a dense rock structure.

Cluster IV (Lhoknga-Lhoong area)

Cluster IV (Lhoknga-Lhoong area) is located in the western part of the Aceh fault, and the subsurface sediments in this area contain alluvium and limestone. The geological formations, such as the Raba Limestone (Murl), Lhoknga Formation (Mul), and Peunasu Formation (Tlp), were formed from the Late Jurassic to the Early Cretaceous. The values of Vs_{30} suggest that the soil in the Lhoknga-Lhoong cluster is categorized class E–D, with low–moderate amplification value, moderate–high dominant frequency, and low Vs_{30}. The moderate–high value range is mainly influenced by the density of the rock structures scattered along the Aceh fault. The vulnerability index in the Lhoknga-Lhoong cluster is relatively low because of the linear relationship between amplification and frequency. Moreover, an active fault passes through this cluster, and thus, mitigation measures must be implemented to reduce destructive effects in the future. No major event has been recorded in the last 170 years in the Aceh segment, but major earthquakes remain possible (Ito *et al.*, 2012).

Cluster V (Seulawah)

The Seulawah cluster is located in the central part of Seulimeum is and close to the Seulawah Agam stratovolcano zone. Most of the rock structures in Lam Teuba Volcanism (QTvt) contain volcanic rocks, formed since the Holocene. The dominant parameter shows high frequency recordings because the rock material is dense and provides low amplification. This soil is class C and is allowed for high construction though other parameters, such as the peak ground acceleration, or possible earthquake intensity. The Vs_{30} is also high, indicating that the subsurface soil properties may support basic construction. This cluster stands on the active Seulimeum fault that moves at a ~2 cm/year slip rate and can produce earthquakes with magnitudes of up to M 7.0. The Seulimeum earthquake in 1930 inflicted significant damages and resulted in many fatalities. This cluster can also be associated with the Seulawah stratovolcano, reported being active in 1839, 1975, and 2010. Volcanic tremors can also be triggered by microseismicity in the central part of the Seulimeum fault.

CONCLUSION

The combination of shear wave velocity, determined by the Spatial Autocorrelation method and parameters of dominant frequency and seismic amplification derived from Horizontal-to-Vertical Ratio, was used to classify the soil properties beneath the northernmost Sumatra, one of the most seismically active regions. The clusters classified from the variation of geophysical data coincide well with geological properties from previous research and studies. Five different clusters representing various types of rocks were classified based on three different seismic properties recorded from the microtremor study at 36 points, covering the sedimentary basin, the active faults, and the Banda Aceh city and its surroundings. The highly populated Banda Aceh city (Cluster I) is among the most vulnerable areas because it stands on a thick sedimentary basin characterized by high amplification and low shear wave velocity. The low-velocity values in Banda Aceh indicate the soft soil types of rock, as observed by the previous study using the Cone Penetration Tests. Therefore, a detailed investigation is required before constructing large and high-altitude infrastructure in Banda Aceh. Cluster II (Jantho) and III (Krueng Raya) are the second most vulnerable areas because the regions are characterized by moderate shear wave

velocity and seismic amplification and are located along the Sumatran and the Seulimeum faults, respectively. The limestone is exposed in Cluster IV, correlating well to the moderate value of Vs and low amplification. Although the Seulawah volcanic region (Cluster V) is categorized by high shear wave velocity, low frequency and low seismic amplification, it is also considered a vulnerable area since it is located along the Seulimeum active fault. The sedimentary layer between the two active faults is imaged by low shear wave velocity along the three vertical profiles. The lateral variation of each geophysical property was mapped by interpolating the wide distance data points at the unsampled locations so that the anomalies between the data points could be missed. However, the research results provide a good picture of the regional structure. A comprehensive study with denser measurement points for Vs and HVSR needs to be conducted to better describe the properties of rocks. The detailed survey and analysis will support the currently available and less-resolution geological map of the study area.

AUTHOR CONTRIBUTIONS

Y. Asnawi contributed in conducting field experiment, HVSR data analysis and drafting the manuscript. A. Simanjuntak performed SPAC data analysis, produced maps and figures as well as interpreted the results. U. Muksin is the corresponding author and the leader of the project who provided funding for the project. S. Putri involved in data acquisition and SPAC data analysis. M. Okubo performed SPAC data analysis and wrote Method part of the manuscript and provided funding supported JSPS KAKENHI. S. Rizal supervised the field experiment and data analysis as well as provided critical revision of the manuscript. M. Syukri supervised the data acquisition in the field and data analysis.

ACKNOWLEDGEMENT

This scientific collaboration between Indonesian and Japanese scientists was supported by JSPS KAKENHI under grant number [17H04577] and Doctoral Dissertation Research Program under grant number [66/UN11.2.1/PT.01.03/DPRM/2021].

CONFLICT OF INTEREST

The authors declare no potential conflict of interest regarding the publication of this work. In addition, the ethical issues including plagiarism, informed consent, misconduct, data fabrication and, or falsification, double publication and, or submission, and redundancy have been completely witnessed by the authors.

OPEN ACCESS

This article is licensed under a Creative Commons Attribution 4.0 International License, which permits use, sharing, adaptation, distribution and reproduction in any medium or format, as long as you give appropriate credit to the original author(s) and the source, provide a link to the Creative Commons license, and indicate if changes were made. The images or other third-party material in this article are included in the article's Creative Commons license, unless indicated otherwise in a credit line to the material. If material is not included in the article's Creative Commons license and your intended use is not permitted by statutory regulation or exceeds the permitted use, you will need to obtain permission directly from the copyright holder. To view a copy of this license, visit: http://creativecommons.org/licenses/by/4.0/

PUBLISHER'S NOTE

GJESM Publisher remains neutral with regard to jurisdictional claims in published maps and institutional affiliations.

ABBREVIATIONS

%	Percentage value
°C	Degree in Celsius
0–10 m	Depth between 0 – 10 m
0°	Azimuth angle in 0 degree
10–20 m	Depth between 11 – 20 m
1D	1-Dimension profile
20–30 m	Depth between 21 – 30 m
A	Amplification
A	Amplitude
A-B	Line of cross section from A to B
A^2	Square of the amplification
AB04	04th observation Point
AB05	05th observation Point
AB09	09th observation Point

AB13	13th observation Point
AB22	22th observation Point
AB23	23th observation Point
AB27	27th observation Point
AVs	Average shear velocity
AVs_{10}	Average shear velocity at 0 – 10 m
AVs_{20}	Average shear velocity at 11 – 20 m
AVs_{30}	Average shear velocity at 21 – 30 m
B	Bandwidth coefficient
BIDO2	SPAC analysis program
Bits	Bit per sample
c	Phase velocity
C	Soil class for sediment – Rock
C-D	Line of cross section from C to D
Cm	Centimetre
cm/year	Centimetre over year
D	Soil class for sediment
DSS	Decision Support System
E	Soil class for soft sediment
E-D	Soil class between soft sediment and hard soil
E-F	Line of cross section from E to F
e.g.	Latin phrase example gratia (for example)
Eq	Equation
EW	Spectrum amplitude in the horizontal east-west component
EW	East-west
F	Frequency
f	Dominant frequency
Fig.	Figure
H/V	The horizontal-to-vertical spectrum
H/V peak	Maximum peak of horizontal-to-vertical spectrum
HVSR	Horizontal to vertical spectral ratio
Hz	Hertz
i.e.	Latin phrase Id est (this is)
Idi	Idi Formation
K	Wavenumber
K_g	Seismic vulnerability index
Km	Kilometre
M	Meter
M	Magnitude
m/s	Meter per second
min.	Minute
Ms	Millisecond
Mul	Lhoknga formation
Murl	Lhoknga limestone rock
NEHRP	National Earthquake Hazards Reduction Program
NS	Spectrum amplitude in the horizontal north–south component
NS	North-South
NW	North-West
Qh	Alluvial sediment structure
QTps	Seulimeum formation
Qtvt	Lam Teuba Volcanic
Rk	Radius between geophone
rk_{max}	Maximum radius between geophone
S	Second
SPAC	Spatial autocorrelation
sps	Sampling per second
STA/LTA	Ratio between the amplitude
SW	South-West
T	Period
Tim	Meucampi formation
Tlp	Peunasu formation
Tuic	Jantho complex formation
USD	United State Dollar
V	Spectrum amplitude in the vertical component of seismic waveform
V/m	Seismometer sensitivity (volt/meter)
Vp	Velocity of pressure
Vs	Share velocity

$Vs_{(0\text{-}10\ m)}$	Shear wave velocities for depths of 0–10 m
$Vs_{(11\text{-}20\ m)}$	Shear wave velocities for depths of 11–20 m
$Vs_{(21\text{-}30\ m)}$	Shear wave velocities for depths of 21–30 m
Vs_{10}	Shear wave velocities for depths of 0–10 m
Vs_{20}	Shear wave velocities for depths of 11–20 m
Vs_{30}	Shear wave velocities for depths of 21–30 m
Z	Vertical Component
π	Pi is a mathematical constant (3,14159)

REFERENCES

Alamri, A.M.; Bankher, A.; Abdelrahman, K.; El-Hadidy, M.; Zahran, H., (2020). Soil site characterization of Rabigh City, western Saudi Arabia coastal plain, using HVSR and HVSR inversion techniques. Arab. J. Geosci., 13(2): 1- 16 (**16 pages**).

Arai, H.; Tokimatsu, K., (2005). S-wave velocity profiling by joint inversion of microtremor dispersion curve and horizontal-to-vertical (H/V) spectrum. Bull. Seismol. Soc. Am., 95(5): 1766–1778 (**13 pages**).

Asrillah, A.; Marwan, M.; Muksin, O.; Ibnu, R.; Takao, S.; Yoshinori, F.; Yuichiro, M.; Hikime, C., (2019). Estimation of vs structure of Krueng Aceh and its suburb basin of Aceh Province, Indonesia. Derived from microtremor measurements. Geosciences. 1–12 (**12 pages**).

Asten, M.W.; Askan A.; Ekincioglu E.E.; Sisman F.N.; Ugurhan B., (2014). Site characterisation in north-western turkey based on SPAC and HVSR analysis of microtremor noise. Explor. Geophys., 45(2): 74–85 (**12 pages**).

Barber, A.J.; Crow, M.J.; J. S. Milsom, (2005). Sumatra: geology, resources and tectonic evolution. J. Geol. Soc., 31 (**282 pages**).

Beroya-Eitner, M.A.; Aydin A.; Tigloa R.; Lasala M., (2009). Use of microtremor in liquefaction hazard mapping. Eng. Geol., 107: 140–153 (**14 pages**).

Bilham, R., (2009). The seismic future of cities. Bull. Earthquake Eng., 7(4): 839–887 **(49 pages)**.

Boore, D.M., (2004). Estimating Vs (30) (or NEHRP site classes) from shallow velocity models (Depths < 30 m). Bull. Seismol. Soc. Am, 94: 591–597 (**7 pages**).

Chávez-García, F.J.; Kang, T.S., (2014). Lateral heterogeneities and microtremors: limitations of HVSR and SPAC based studies for site response. Eng. Geol., 174: 1–10 **(10 pages)**.

Cho, I., (2019). Two-sensor microtremor SPAC method: potential utility of imaginary spectrum components. Geophys. J. Int., 220(3): 1735-1747 (**13 pages**).

Cho, I.; Tada, T.; Shinozaki, Y., (2004). A new method to determine phase velocities of Rayleigh waves from microseisms. Geophysics. 69(6): 1535–1551 (**17 pages**).

Cho, I.; Tada, T.; Shinozaki, Y., (2006). Centerless circular array method: inferring phase velocities of rayleigh waves in broad wavelength ranges using microtremor records. J. Geophys. Res.: Solid Earth. 111(9): 1-12 (**12 pages**).

Cho, I.; Tada, T.; Shinozaki, Y., (2008). A new method of microtremor exploration using miniature seismic arrays: quick estimation of average shear velocities of the shallow soil. Butsuri-Tansa Geophys. Explor., 61(6): 457–468 (**12 pages**).

Claprood, M.; Asten, M.W.; Kristek, J., (2012). Combining HVSR microtremor observations with the SPAC method for site resonance study of the Tamar Valley in Launceston. Geophys. J. Int., 191(2): 765-780 (**16 pages**).

Culshaw, M.G.; Duncan, S.V.; Sutarto, N.R., (1979). Engineering geological mapping of the Banda Aceh alluvial basin, Northern Sumatra, Indonesia. Bull. Int. Assoc. Eng. Geol., 19(1): 40–47 (**8 pages**).

El-Hady, S.; Ferqany, E.AA.; Othman, A.; Mohamed, G.E.A., (2012). Seismic microzonation of Marsa Alam, Egypt using inversion HVSR of microtremor observations. J. Seismolog., 16(1): 55–66 (**12 pages**).

Forte, G.; Chiocarelli, E.; De Falco, M; Cito, P.; Santo, A.; Lervolino, I., (2019). Seismic soil classification of Italy based on surface geology and shear-wave velocity measurements. Soil Dyn. Earthquake Eng., 122:79–93 (**15 pages**).

Gallipoli, M.R.; Mucciarelli, M.; Galliaccio, S.; Tropeano, M.; Lizza, C., (2004). Horizontal to vertical spectral ratio (HVSR) measurements in the area damaged by the 2002 Molise, Italy, earthquake. Earthquake Spectra. 20(SPEC. 1): 81-93 (**13 pages**).

Goda, K.; Kiota, T.; Fokhrel, R.M.; Chiaro, G.; Katagiri, T.; Sharma, K.; Wilkinson, S., (2015). The 2015 Gorkha Nepal earthquake: insights from earthquake damage survey. Front. Built Environ., 1(8): (**15 pages**).

Gosar, A., (2007). Microtremor HVSR study for assessing site effects in the bovec basin (nw slovenia) related to 1998 Mw5.6 and 2004 Mw5.2 earthquakes. Eng. Geol., 91(2–4): 178–193 (**16 pages**).

Hollender, F.; Cornou, C.; Deschamp, A.; Oghalaei, K.; Renalier, F.; Moufroy, E.; Burnouf, C.; Thomassin, S.; Wathelet, M.; Bard, PY.; Boutin, V.; Desbordes, C.; Isabelle, DB.; Foundotos, L.; Cedric, GB.; Perron, V.; Regnier, J.; Roulle, A.; Langlais, M.; Sicillia, D., (2018). Characterization of site conditions (soil class, VS30, velocity profiles) for 33 stations from the French permanent accelerometric network (RAP) using surface-wave methods. Bull. Earthquake Eng., 16(6): 2337–2365 (**29 pages**).

Idris, Y.; Cummims, P.; Rusydy, I.; Muksin, U.; Syamsidik; Habibie, M.Y.; Meilanda, E., (2019). Post-earthquake damage assessment after the 6.5 Mw earthquake on December, 7th 2016 in Pidie Jaya, Indonesia. J. Earthquake Eng., 1–18 (**18 pages**).

Ito, T.; Gunawan, E.; Kimata, F.; Tabai, T. Simons, M.; Meilano, I.; Agustan; Ohta, Y.; Nurdin, I.; Sugiyanto, D., (2012). Isolating along-strike variations in the depth extent of shallow creep and fault locking on the northern Great Sumatran Fault. J. Geophys. Res. 117(510): 1–16 (**16 pages**).

Jalil, A.; Fathani, T.F.; Satyarno, I.; Wilopo, W., (2020). A study on the Liquefaction potential in Banda Aceh city after the 2004 Sumatera earthquake. International Journal of GEOMATE, 18: 147-155 (**9 pages**).

Kanli, A.I.; Tildy, P.; Pronay, Z.; Pinar, A.; Hermann, L., (2006). Vs30 mapping and soil classification for seismic site effect evaluation in Dinar Region, SW Turkey. Geophys. J. Int., 165(1): 223–235 (**13 pages**).

Maresca, R.; Nardone, L.; Gizzi, F. T.; Potenza, M. R., (2018). Ambient noise HVSR measurements in the Avellino Historical Centre and surrounding area (Southern Italy). Correlation with surface geology and damage caused by the 1980 Irpinia-Basilicata earthquake. Measurement. 130: 211–222 (**12 pages**).

Matsuoka, M.; Wakamatsu, K.; Fujimoto, K.; Midorikawa, S., (2006). Average shear-wave velocity mapping using Japan engineering geomorphologic classification map. Structural Engineering/Earthquake Engineering, 23(1): 58-67 (**10 pages**).

Muksin, U.; Irwandi; Rusydy, I.; Muzli; Erbas, K.; Marwan; Asrillah; Muzakir; Ismail, N., (2018). Investigation of Aceh segment and Seulimeum fault by using seismological data; A preliminary result. J. Phys. Conf. Ser., 1011(1): (**5 pages**).

Muksin, U.; Bauer, K.; Muzli, M.; Ryberg, T.; Nurdin, I.; Masturiyono, M.; Weber, M., (2019). AcehSeis project provides insights into the detailed seismicity distribution and relation to fault structures in Central Aceh, Northern Sumatra. J. Asian Earth Sci., 171: 20–27 (**8 pages**).

Muzli, M.; Muksin, U.; Nugraha, A. D.; Bradley, K. E.; Widiyantoro, S.; Erbas, K.; Jousset, P.; Rohadi, S.; Nurdin, I.; Wei, S., (2018). The 2016 Mw 6.5 Pidie Jaya, Aceh, North Sumatra, earthquake: Reactivation of an unidentified sinistral fault in a region of distributed deformation. Seismol. Res. Lett., 89(5): 1761–1772.

Nakamura, Y. (1989)**.** A method for dynamic characteristics estimation of subsurface using microtremor on the ground surface**.** Railway Tech. Res.Institute, Quarterly Reports, 30(1): 25–33 (**9 pages**).

Nakamura, Y. (1997)**.** Seismic vulnerability indices for ground and structures using microtremor**.** World congress on railway research in Florence, Italy. 16–19 (**4 pages**).

Nakamura, Y. (2000)**.** Clear identification of fundamental idea of Nakamura's technique and its applications. In proceedings of the 12th world conference on earthquake engineering. New Zealand: Auckland. Vol. 2656 (**8 pages**).

Nakamura, Y. (2009)**.** Basic structure of QTS (HVSR) and examples of applications. In increasing seismic safety by combining engineering technologies and seismological data. Springer, Dordrecht. 33–51 (**19 pages**).

Okada, H. (2006). Theory of efficient array observations main of microtremors with special reference to the SPAC method. Explor. Geophys., 59(1): 73–85 (**13 pages**).

Pamuk, E.; Özdag. Ö.C.; Tuchel, A.; Özyalin, S.; Akgun, M., (2018). Local site effects evaluation for Aliağa/İzmir using HVSR (Nakamura technique) and MASW methods. Nat. Hazards. 90(2): 887–899 (**13 pages**).

Park, C.B.; Miller, R.D.; Xia, J., (2007). Multichannel analysis of surface waves (MASW). Geophysics, 64(3): 800–808 (**9 pages**).

Parker, R.N.; Hancox, G.T.; Petley, D.N.; Messey, C.I.; Densmore, A.L.; Rosser, J.N., (2015). Spatial distributions of earthquake-induced landslides and hillslope preconditioning in the northwest South Island, New Zealand. Earth Surf. Dyn., 3(4): 501–525 **(25 pages)**.

Rahman, M.Z.; Kamal, A.S.M.M.; Siddiqua, S., (2018). Near-surface shear wave velocity estimation and V s30 mapping for Dhaka City, Bangladesh. Nat. Hazards. 92(3): 1687–1715 (**29 pages**).

Rusydy, I.; Muksin, U.; Mulkal; Idris, Y.; Akram, M.N.; Syamsidik, (2018). The prediction of building damages and casualties in the Kuta Alam sub district-Banda Aceh caused by different earthquake models. AIP Conf. Proc., 1987, 020012: (**7 pages**).

Rusydy, I.; Idris, Y.; Mulkal; Muksin, U; Cummins, P.; Akram, M.N.; Syamsidik, (2020). Shallow crustal earthquake models, damage, and loss predictions in Banda Aceh, Indonesia. Geoenviron. Disasters, 7(8): 1-16 (**16 pages**).

Ryberg, T.; Muksin, U.; Bauer, K., (2016). Ambient seismic noise tomography reveals a hidden caldera and its relation to the Tarutung pull-apart basin at the Sumatran fault zone, Indonesia. J. Volcanol. Geotherm. Res., 321: 73–84 (**12 pages**).

Scott, J.B.; Rasmussen, T.; Luke, B.; Taylor, W.J.; Wagober, J.L.; Smith, S.B.; Louie, J.N., (2006). Shallow shear velocity and seismic microzonation of the urban Las Vegas, Nevada, basin. Bull. Seismol. Soc. Am., 96(3): 1068–1077 (**10 pages**).

Sieh, K.; Natawidjaja, D., (2000). Neotectonics of the Sumatran fault, Indonesia. J. Geophys. Res.: Solid Earth, 105(B12): 28295–28326 (**32 pages**).

Siemon, B.; Steuer, A., (2010). Airborne geophysical investigation of groundwater resources in northern Sumatra after the tsunami of 2004. The Tsunami Threat - Research and Technology, (May 2014): 575-594 (**20 pages**).

Stanko, D.; Markusic, S.; Strelec, S.; Gazdek, M., (2017) "Equivalent-linear site response analysis on the site of the historical Trakošćan Castle, Croatia, using HVSR method," Environ. Earth Sci., 76:642 (**21 pages**).

Thein, P.S.; Pramumijoyo, S.; Brotopuspito, K.S.; Kiyono, J.; Wilopo, W.; Furukawa, A.; Setianto, A.; Putra, R.R., (2015). Estimation of S-wave velocity structure for sedimentary layered media using microtremor array measurements in Palu City, Indonesia. Procedia Environ. Sci., 28(Sustain, 2014): 595–605 (**11pages**).

Tohari, A.; Sugianti, K.; Syahbana, A.J.; Soebowo, E., (2015). Cone penetration test (CPT)-based liquefaction susceptibility of Banda Aceh city, RISET Geologi dan Pertambangan, 25, 99-110 (**12 pages**).

Tün, M.; Pekkan, E., Ozel, O.; Guney, Y., (2016). An investigation into the bedrock depth in the Eskisehir quaternary basin (Turkey) using the microtremor method. Geophys. J. Int., 207(1): 589–607 (**19 pages**).

Untung M.; Buyung N.; Kertapati E.; Undang; Allen C.R., (1985). Rupture along the Great Sumatran Fault, Indonesia, the earthquakes of 1926 and 1943. Bull. Seismol. Soc. Am., 75(1): 313–317 **(4 pages).**

AUTHOR (S) BIOSKETCHES

Asnawi, Y., Ph.D. Candidate, Assistant Professor, [1]Graduate School of Mathematics and Applied Sciences, Universitas Syiah Kuala, Banda Aceh 23111, Indonesia. [2]Universitas Islam Negeri Ar-Raniry, Banda Aceh 23111, Indonesia. [3]Tsunami and Disaster Mitigation Research Center, Universitas Syiah Kuala, Jl. Prof. Dr. Ibrahim Hasan, Gampong Pie, Indonesia.
- Email: *yusran@ar-raniry.ac.id*
- ORCID: 0000-0003-0806-1716
- Web of Science ResearcherID: NA
- Scopus Author ID: 57217127838
- Homepage: http://tdmrc.unsyiah.ac.id/

Simanjuntak, A.V.H., Ph.D. Candidate, Tsunami and Disaster Mitigation Research Center, Universitas Syiah Kuala, Jl. Prof. Dr. Ibrahim Hasan, Gampong Pie, Indonesia. [4]Meteorological, Climatological, and Geophysical Agency, BMKG, Banda Aceh 23234, Indonesia.
- Email: *andreansimanjuntak@gmail.com*
- ORCID: 0000-0003-0623-0037
- Web of Science ResearcherID: NA
- Scopus Author ID: 57195483722
- Homepage: http://tdmrc.unsyiah.ac.id/

Muksin, U., Ph.D., Associate Professor, Tsunami and Disaster Mitigation Research Center, Universitas Syiah Kuala, Jl. Prof. Dr. Ibrahim Hasan, Gampong Pie, Indonesia.
- Email: muksin.umar@tdmrc.org
- ORCID: 0000-0001-7297-8065
- Web of Science ResearcherID: W-3934-2018
- Scopus Author ID: 55795600300
- Homepage: http://fsd.unsyiah.ac.id/muksinumar/

Okubo, M., Ph.D., Associate Professor, Natural Science Cluster, Science and Technology Unit, Kochi University, Akebono-cho Kochi, Japan.
- Email: *okubo@kochi-u.ac.jp*
- ORCID: 0000-0001-7784-6053
- Web of Science ResearcherID: NA
- Scopus Author ID: 8641817600
- Homepage: https://www.kochi-u.ac.jp/english/academics/science/

Putri, S.I., B.Sc., Tsunami and Disaster Mitigation Research Center, Universitas Syiah Kuala, Jl. Prof. Dr. Ibrahim Hasan, Gampong Pie, Indonesia.
- Email: *izziaputris@gmail.com*
- ORCID: 0000-0001-9331-0099
- Web of Science ResearcherID: NA
- Scopus Author ID: NA
- Homepage: http://tdmrc.unsyiah.ac.id/

Rizal, S., Ph.D., Professor, Graduate School of Mathematics and Applied Sciences, Universitas Syiah Kuala, Banda Aceh 23234, Indonesia.
- Email: *syamsul.rizal@unsyiah.net*
- ORCID: 0000-0002-7691-9449
- Web of Science ResearcherID: V-7627-2017
- Scopus Author ID: 56950902200
- Homepage: http://fsd.unsyiah.ac.id/syamsul_rizal/

Syukri, M., Ph.D., Professor, Graduate School of Mathematics and Applied Sciences, Universitas Syiah Kuala, Banda Aceh 23234, Indonesia.
- Email: *m.syukri@unsyiah.ac.id*
- ORCID: 0000-0003-0405-3145
- Web of Science ResearcherID: NA
- Scopus Author ID: 57217853545
- Homepage: http://fsd.unsyiah.ac.id/m.syukri/

HOW TO CITE THIS ARTICLE

Asnawi, Y.; Simanjuntak, A.; Muksin, U.; Okubo, M.; Putri, S.I.; Rizal, S.; Syukri, M., (2022). Soil classification in a seismically active environment based on shear wave velocity and HVSR data. Global J. Environ. Sci. Manage., 8(3): 297-314.

DOI: 10.22034/gjesm.2022.03.01

url: https://www.gjesm.net/article_247726.html